breaks the antiferromagnetic coupling will increase the moment, while lowering λ will tend to decrease the moment since all these complexes contain octahedral Co^{II}. Both of these effects are operative in these compounds.

The differences in magnetic moments between the 0e and 2e blue species vary depending on the field. If no coupling is present (as is the case in $Co^{II}W_{11}Co^{II}$ at 70 500 G where the antiferromagnetic coupling has been completely broken, giving the maximum expected moment of 6.80 μ_B), the 2e reduction should affect the tetrahedral and octahedral Co atoms independently. That is indeed the result observed in $Co^{II}W_{11}Co^{II}$2e at 70 500 G since the moment is decreased considerably upon reduction as would be expected for an isolated octahedral Co^{II} (see Table IV). At 5000 G, however, the moment remains practically constant upon reduction. Since the Co–Co magnetic coupling is known to be operative at this field,[18,19,27] an invariant moment implies cancellation of two effects: (1) a lowering of the moment upon reduction because of decreased orbital contribution from octahedral Co^{II} and (2) an increase of the moment owing to the partial or total breaking of the magnetic coupling between the cobalts.

This interpretation is supported by the $Fe^{III}W_{11}Co^{II}$ case, which shows an increase in moment upon reduction at both fields, suggesting that the effect of breaking the coupling (itself larger than in the Co–Co case)[18,19] by the 2e reduction is greater than the effect of lowering the spin–orbit coupling of octahedral Co^{II}.

As expected from the fact that the Fe^{III}–Co^{II} interaction is stronger than the Co^{II}–Co^{II} interaction, the 70 500 G field does not break completely the antiferromagnetic coupling in the former, changing μ_{eff} only from 6.14 to 6.45 μ_B (vs a 7.7 μ_B maximum) in the oxidized form and from 6.36 to 6.63 μ_B in the 2e blue.

The temperature dependences in the cases of $Co^{II}W_{11}Co^{II}$2e and $Co^{II}W_{11}Co^{II}$ (Figure 6) show that at high temperatures the blue is slightly more paramagnetic than the oxidized complex, while at low temperatures the reverse is true. This shows that the temperature dependences of variation in spin–orbit coupling and in degree of breaking of the antiferromagnetic coupling are not the same. In fact, the breaking of the Co–Co coupling in the 2e blue must be the larger factor above about 100 K at this applied field, while the lowering of λ by the reduction must be the larger factor below about 100 K.

$Fe^{III}W_{11}Co^{II}$2e shows, over the whole temperature range, greater paramagnetism than its oxidized parent, having therefore a lower Fe^{III}–Co^{II} coupling at all times. However, the difference between the oxidized and 2e blue increases with temperature, which may be explained by the lowering of the antiferromagnetic coupling being greater than the lowering of λ despite the fact that both effects may be decreasing as the temperature is lowered.

It is interesting to note from comparison of the Fe–Co and Co–Co cases that the M–M coupling is lowered more effectively upon reduction in the case for which $|J|$ was much larger before reduction. It is probable that the ring currents in the blue species modify superexchange pathways in specific directions and that this modifies effective J's.

It will be highly desirable to extend this study to other species to cover a broader range of effects. Complexes containing (1) two ions with positive λ values, (2) more than one paramagnetic atom in octahedral sites, or (3) ferromagnetically coupled atoms are among the possibilities.

Acknowledgment. We thank Prof. Ekkehard Sinn for making available the SHE SQUID magnetometer at UVA and Dr. Thitinant N. Thaniasiri for help in its use. This research was supported by NSF Grant No. CHE-8406088, by an instrument grant from the W.M. Keck Foundation, by the U.S.–Spain Joint Committee for Scientific Cooperation through Grant No. CCB-8504039, and through a fellowship for N.C.-P.

β-Migratory Insertion Reactions of $(\eta^5\text{-}C_5R'_5)Rh(L)(C_2H_4)R^+BF_4^-$ (R′ = H, CH_3; R = H, C_2H_5; L = $P(OMe)_3$, PMe_3). Comparison of the Energetics of Hydride versus Alkyl Migration

Maurice Brookhart,* Elisabeth Hauptman, and David M. Lincoln

Contribution from the Department of Chemistry, University of North Carolina, Chapel Hill, North Carolina 27599-3290. *Received June 18, 1992. Revised Manuscript Received September 14, 1992*

Abstract: Protonation of the rhodium ethylene complexes $C_5R_5(L)Rh(C_2H_4)$, **1a,b** and **2a,b** (**1** R = CH_3, **2** R = H, **a** L = $P(OMe)_3$, **b** L = PMe_3), with $HBF_4 \cdot Me_2O$ in CH_2Cl_2 yields the four corresponding ethylene hydride complexes $C_5R_5(L)Rh(C_2H_4)H^+$, **3a,b** and **4a,b**. NMR techniques were used to measure the rates of migratory insertion for these species. Values for the free energies of activation were found to be 12.2 (**3a**), 12.1 (**3b**), 15.0 (**4a**), and 15.0 (**4b**) kcal/mol. Eyring plots based on rate constants measured over the −20 to +20 °C range established $\Delta S^\ddagger = 0$ for these migratory insertions. Treatment of **3a,b** and **4a,b** with excess ethylene gave the ethyl ethylene complexes $C_5R_5(L)RhCH_2CH_3(C_2H_4)^+$, **7a,b** and **8a,b**, whose structures were established by ^1H and ^{13}C NMR spectroscopy. These complexes function as ethylene dimerization catalysts; NMR spectroscopic analysis of the catalytic systems shows that **7a,b** and **8a,b** are the catalyst resting states. The turnover-limiting step is the β-migratory insertion reaction of the ethyl ethylene complexes. The $\Delta G^\ddagger$ values for β-migratory insertion calculated from turnover rates were found to be 22.4 (**7a**), 23.4 (**7b**), 23.4 (**8a**), and 24.7 (**8b**) kcal/mol. The $\Delta\Delta G^\ddagger$ values for H versus CH_2CH_3 migration for these systems thus lie in the range of 8.5–11 kcal/mol, which corresponds to relative migratory aptitudes k_H/k_{Et} of 10^6–10^8 at 23 °C.

The β-migratory insertion of transition metal olefin hydride complexes is a fundamental transformation of importance in several catalytic processes, including olefin hydrogenations, hydroformylations, and isomerizations. The analogous β-migratory insertion reaction of metal alkyl olefin complexes is the key carbon–carbon bond forming step in metal-catalyzed olefin polymerization reactions and related oligomerizations and dimerizations.[1]

0002-7863/92/1514-10394$03.00/0

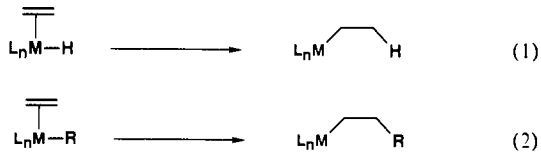

Numerous stable olefin hydride complexes have been isolated and characterized. The kinetics of the migratory insertion reactions for many of these species have been examined primarily using NMR techniques to determine the rate of exchange between the metal hydride and the olefinic hydrogens.[2-9] Electronic and steric effects have been probed using substituted olefins, and the nature of the transition state has been considered.[2a,c,8] Similarly, rates of exchange of the agostic hydrogen and β-hydrogens in species of the general type $L_nMCH_2CH_2\text{-}\mu\text{-}H$ have also been examined using NMR techniques.[10-13]

Insertion reactions of alkenes into the metal–carbon bond of unsaturated d^0 metal alkyl species have been studied extensively since electrophilic d^0 species are clearly the active intermediates in Ziegler–Natta catalytic systems.[14] The precise nature of the transition state for insertion is still under debate but may involve species with an α-agostic C–H interaction at least in some systems.[14b,f] No olefin alkyl complexes have ever been observed as intermediates in these d^0 systems.

In d^n systems when $n > 0$, several stable alkyl olefin complexes have been isolated; however, many of these complexes do not exhibit β-migratory insertion reactions presumably due to high kinetic barriers.[2b,6a,15-20] In two systems, $CpNi(C_2H_4)R$[17] and $C_5R_5Co(C_2H_4)(CH_3)_2$ (R = CH_3, H),[16a,b] direct evidence for the β-migratory insertion reaction (eq 2) was obtained, but no activation barriers were determined. Most recently, Flood has reported the migratory insertion of η^3-(1,4,7-trimethyl-1,4,7-triazacyclononane)$Rh(CH_3)_2(C_2H_4)^+$, which exhibits E_a = 19 kcal/mol.[19] In these systems the analogous hydride species were unavailable for study.

Table I. Selected ^1H and ^{13}C NMR Data for **3** and **4**

compd[a] (T, °C)	H	$C_{\alpha \text{ or } \beta}$	$C_{\alpha \text{ or } \beta}$	J_{RhH}, Hz	J_{PH}, Hz
3a (−94)	−9.95	54.6[b]	53.4[b]	18	18
3b (−80)	−10.7	51.7	49.2	18	31
4a (−114)	−9.94	48.3	47.1	15	15
4b (−92)	−10.5	47.0	46.0	18	25

[a] All spectra were recorded in CD_2Cl_2. Chemical shifts are in ppm relative to TMS taken as 0 ppm. [b] Recorded in acetone-d_6.

It was the aim of this work to identify a set of complexes where the β-migratory insertion reactions of both the hydride and alkyl olefin complexes could be examined and quantitatively compared. Such studies would then provide insight into the relative migratory aptitudes of H versus R in β-migratory insertion reactions. Furthermore, although relative migratory aptitudes will vary from system to system, such quantitative information will provide at least qualitative guidelines for predicting rates of alkyl migrations based on the normally more readily obtained rates of hydride migration. We describe here kinetic studies of the β-migratory insertion reactions of the hydride complexes $C_5R_5(L)Rh(C_2H_4)(H)^+$ and the analogous ethyl complexes $C_5R_5(L)Rh(C_2H_4)(Et)^+$ (R = H, CH_3; L = $P(OMe)_3$, PMe_3) which establish migratory aptitudes of H versus C_2H_5 in these systems. Part of this work has been previously reported.[9] Subsequent to these studies, we have also determined the rate of β-migratory insertion in ethylene polymerization intermediates of the type $Cp^*(P(OMe)_3)Co(C_2H_4)R^+$ and have compared this rate to the rate of exchange of the agostic hydrogen with the β-hydrogens in $Cp^*(P(OMe)_3)CoCH_2CH_2\text{-}\mu\text{-}H^+$.[18]

Results and Discussion

A. Generation, Spectral Characterization, and Dynamics of the Ethylene Hydride Complexes $C_5R_5(L)Rh(C_2H_4)(H)^+$ (R = Me, H; L = $P(OMe)_3$, PMe_3; 3 and 4). 1. Hydride Generation and Low-Temperature NMR Spectroscopic Characterization. The terminal hydride species **3** and **4** were generated by protonation of the neutral ethylene complexes **1** and **2** with $HBF_4\cdot Me_2O$ at low temperatures (ca. −30 °C; for details, see the Experimental Section). All cationic complexes could be isolated as salts except **3b** and **4a**, which were characterized and used in situ. Static ^1H

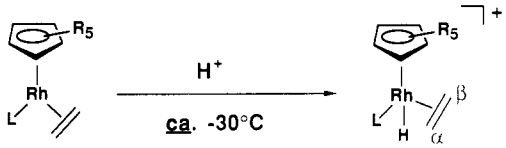

1 R= Me **3** R= Me

2 R= H **4** R= H

L= (a) $P(OMe)_3$ (b) PMe_3

and ^{13}C NMR spectra (250 and 400 MHz) of these species in CD_2Cl_2 were recorded below −70 °C, and key parameters are summarized in Table I. Data for **4b** match that previously reported by Werner.[6b] Complete spectroscopic data are given in the Experimental Section. Definitive evidence for a terminal hydride versus an agostic species comes from the lack of coupling between the rhodium hydride and $^{13}C_\alpha$ or $^{13}C_\beta$ (<4 Hz) and the large values of J_{RhH} and J_{PH} (see Table I). For comparison Werner reported J_{PH} values of 24 and 32 Hz, respectively, for terminal hydrides $CpRh(P(OMe)_3)_2H^+$[21a] and CpRh-

(1) See, for example: (a) Collman, J. P.; Hegedus, L. S.; Norton, J. R.; Finke, R. G. *Principles and Applications of Organotransition Metal Chemistry*; University Science Books: Mill Valley, CA, 1987. (b) Parshall, G. W. *Homogeneous Catalysis*; Wiley: New York, 1980. (c) *Transition Metal Catalyzed Polymerization; Ziegler-Natta and Metathesis Polymerization*; Quirk, R. P., Ed.; Cambridge Press: Cambridge, 1988.

(2) (a) Bercaw, J. E.; Doherty, N. M. *J. Am. Chem. Soc.* **1985**, *107*, 2670. (b) Bercaw, J. E.; Parkin, G.; Bunel, E.; Burger, B. J.; Trimmer, M. S.; Van Asselt, A. *J. Mol. Catal.* **1987**, *41*, 21. (c) Bercaw, J. E.; Burger, B. J.; Santarsiero, B. D.; Trimmer, M. S. *J. Am. Chem. Soc.* **1988**, *110*, 3134.

(3) Osborn, J. A.; Byrne, J. W.; Blaser, H. U. *J. Am. Chem. Soc.* **1975**, *97*, 3871.

(4) Cooper, J. N.; McNally, J. P. *Organometallics* **1988**, *7*, 1704.

(5) Wilkinson, G.; Chaudret, B. N.; Cole-Hamilton, D. J. *Acta Chem. Scand., Ser. A* **1978**, *A32*, 763.

(6) (a) Werner, H.; Werner, R. *J. Organomet. Chem.* **1979**, *174*, C63. (b) Werner, H.; Feser, R. *J. Organomet. Chem.* **1982**, *233*, 193.

(7) Roe, D. C. *J. Am. Chem. Soc.* **1983**, *105*, 7770.

(8) Halpern, J.; Okamoto, T. *Inorg. Chim. Acta* **1984**, *89*, L53.

(9) Brookhart, M.; Lincoln, D. M. *J. Am. Chem. Soc.* **1988**, *110*, 8719.

(10) Brookhart, M.; Green, M. L. H.; Wong, L. *Prog. Inorg. Chem.* **1988**, *36*, 1.

(11) (a) Brookhart, M.; Green, M. L. H.; Pardy, R. B. A. *J. Chem. Soc., Chem. Commun.* **1983**, 691. (b) Brookhart, M.; Schmidt, G. F. *J. Am. Chem. Soc.* **1985**, *107*, 1443. (c) Brookhart, M.; Lincoln, D. M.; Volpe, A. F.; Schmidt, G. F. *Organometallics* **1989**, *8*, 1212.

(12) Bennett, M. A.; McMahon, I. J.; Pelling, S. *J. Organomet. Chem.* **1990**, *382*, 175.

(13) (a) Spencer, J. L.; Cracknell, R. B.; Orpen, A. G. *J. Chem. Soc., Chem. Commun.* **1984**, 326. (b) Spencer, J. L.; Cracknell, R. B.; Orpen, A. G. *J. Chem. Soc., Chem. Commun.* **1986**, 1005. (c) Spencer, J. L.; Conroy-Lewis, F. M.; Mole, L.; Redhouse, A. D.; Litster, S. A. *J. Chem. Soc., Chem. Commun.* **1991**, 1601.

(14) For leading references, see: (a) Watson, P. L. *J. Am. Chem. Soc.* **1982**, *104*, 337. (b) Grubbs, R. H.; Clawson, L.; Soto, J.; Buchwald, S. L.; Steigerwald, M. L. *J. Am. Chem. Soc.* **1985**, *107*, 3377. (c) Marks, T. J.; Jeske, G.; Lauke, H.; Mauermann, H.; Swepston, P. N.; Schumann, H. *J. Am. Chem. Soc.* **1985**, *107*, 8091. (d) Hlatky, G. G.; Turner, H. W.; Eckman, R. R. *J. Am. Chem. Soc.* **1989**, *111*, 2728. (e) Bercaw, J. E.; Burger, B. J.; Thompson, M. E.; Cotter, W. D. *J. Am. Chem. Soc.* **1990**, *112*, 1566. (f) Bercaw, J. E.; Piers, W. E. *J. Am. Chem. Soc.* **1990**, *112*, 9406. (g) Jordan, R. F.; Lapointe, R. E.; Baenziger, N.; Hinch, G. D. *Organometallics* **1990**, *9*, 1539.

(15) Green, M. L. H.; Mahtab, R. *J. Chem. Soc., Dalton Trans.* **1979**, 262.

(16) (a) Bergman, R. G.; Evitt, E. R. *J. Am. Chem. Soc.* **1980**, *102*, 7003. (b) Pardy, R. B. A. *J. Organomet. Chem.* **1981**, *216*, C29.

(17) Lehmkuhl, H. *Pure Appl. Chem.* **1986**, *58*, 495.

(18) Brookhart, M.; Volpe, A. F.; Lincoln, D. M.; Horváth, I. T.; Millar, J. M. *J. Am. Chem. Soc.* **1990**, *112*, 5634.

(19) Flood, T. C.; Wang, L. *J. Am. Chem. Soc.* **1992**, *114*, 3169.

(20) Alkene insertion into a chelated platinum–alkyl bond has been reported: Flood, T. C.; Bitler, S. P. *J. Am. Chem. Soc.* **1984**, *106*, 6076.

$(PMe_3)_2H^+$.[21b] These values are similar to those of **3** and **4** and thus lend support to our assignment of the hydrides as terminal. Much reduced J_{PH} couplings have been noted in comparing agostic species involving phosphine and phosphite complexes with terminal hydride complexes. For example, the J_{PH_a} coupling in $Cp^*(P(OMe)_3)CoCH_2CH_2$-μ-H_a^+ is ca. 12 Hz compared to the J_{PH} of 80 Hz in $Cp^*(P(OMe)_3)_2CoH^+$.[11c] All J_{RhH} values for **3** and **4** fall in a narrow range (15–18 Hz) and are similar to the J_{RhH} coupling constant of 22 Hz for terminal hydrides $CpRh(P(OMe)_3)_2H^+$[21a] and $CpRh(PMe_3)_2H^+$.[21b] It is interesting to note that if L = C_2H_4, the rhodium hydride complex shows a β-H agostic interaction. This clearly indicates that the energy difference between the agostic and terminal hydrides in these systems is small and that the stable form can be controlled by small variations in the ancillary ligands. This change is most simply explained by supposing that the increased π-acidic character of C_2H_4 renders the rhodium center more electrophilic, which favors a bridging M···H···C interaction.

2. Analysis of Dynamic Processes in 3 and 4. Summarized below are two dynamic processes exhibited by the hydride species **3** and **4**. Process I corresponds to ethylene rotation and results in exchange of C_α and C_β as well as H_2 with H_3 and H_1 with H_4. Process II, reversible migratory insertion, results in exchange of H, H_1, and H_2. This process is most easily envisioned as occuring

Process I: Ethylene Rotation

Process II: Hydride Migration

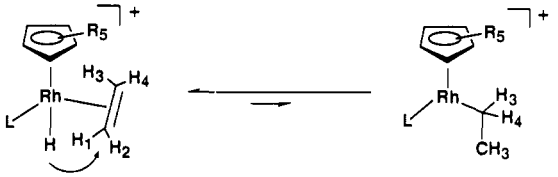

6

through the 16-electron intermediates **6**, but an "in-place" rotation mechanism[22] is also possible. These alternatives are discussed in more detail below. When β-migratory insertion is coupled with the generally faster ethylene rotation process, exchange of all five hydrogens, H and H_1–H_4, occurs.

The rates for process I are most easily measured by line-shape analysis of the ^{13}C signals of C_α and C_β since only ethylene rotation results in their exchange. When process I is much faster than process II, spin saturation transfer experiments can be performed on $H_1 \rightleftharpoons H_4$ or $H_2 \rightleftharpoons H_3$ (details of these dynamic analyses are contained in the Experimental Section).

Rates for β-migratory insertion are most conveniently measured either by (a) line-shape analysis of the Rh–H signals since only process II results in transfer of rhodium hydride to an olefinic site or by (b) spin saturation transfer experiments whereby the Rh–H signal is saturated and the intensity decrease of the olefinic signals is monitored. Both sets of rate determinations yield similar free energies of activation.

In the case of the analysis of the line shapes of the Rh–H resonances, the experimental line shapes were compared to calculated line shapes using the DNMR3 simulation program. Figure 1 illustrates the set of observed and calculated spectra for complex

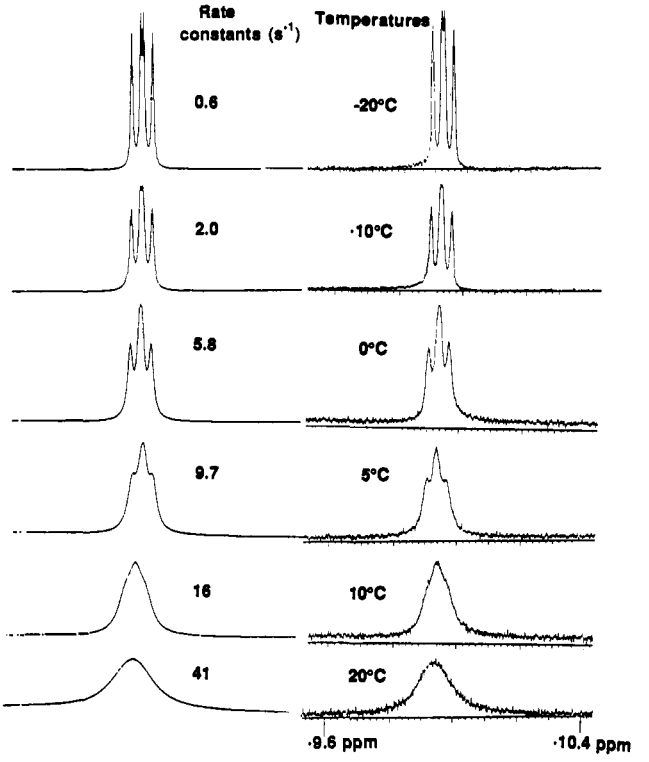

Figure 1. Experimental (right) and calculated (left) ^1H NMR spectra (400 MHz) of the hydride region for **4a**.

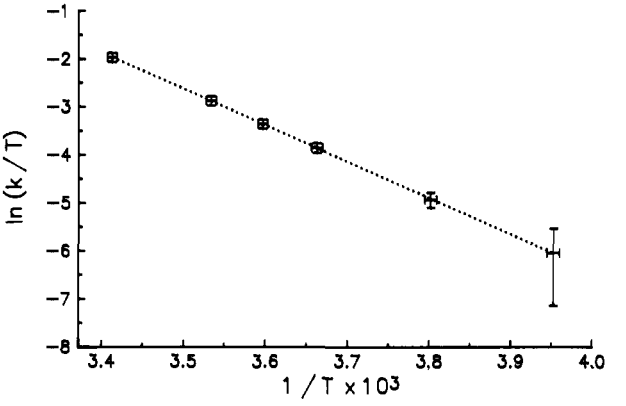

Figure 2. Eyring plot for hydride migration of $CpRhP(OMe)_3(C_2H_4)H^+$ (**4a**).

4a. Using this technique, rate constants could be obtained over a 40 °C temperature range (−20 to 20 °C), which permits calculation of $\Delta H^\ddagger$ and $\Delta S^\ddagger$ for this process. Eyring plots of the data for **4a** and **4b** yield $\Delta H^\ddagger$ = 15.0 ± 1.0 kcal/mol and $\Delta S^\ddagger$ = 0.3 ± 3.0 eu for **4a** and $\Delta H^\ddagger$ = 14.8 ± 1.0 kcal/mol and $\Delta S^\ddagger$ = 0 ± 3.0 eu for **4b**.[23] The Eyring plot for **4a** is shown in Figure 2. As expected for an intramolecular H migration, $\Delta S^\ddagger$ is near 0; thus, $\Delta H^\ddagger \approx \Delta G^\ddagger$. The accuracy of these measurements and the observation that $\Delta S^\ddagger$ is ca. 0 imply that comparisons of $\Delta G^\ddagger$ values at different temperatures can be made and that extrapolation of rate constants over moderate temperature ranges will yield accurate values. The free energies of activation for the dynamic processes described above are listed in Table II. Selected rate constants are presented in the table; additional values are given in the Experimental Section.

The ethylene rotational barriers exhibit two trends: (a) the barriers for the Cp* complexes are ca. 2.5 kcal/mol higher than their Cp analogs, and (b) the barriers in the PMe_3-substituted systems are ca. 1 kcal/mol higher than in the $P(OMe)_3$-substituted

(21) (a) Werner, H.; Neukomm, H.; Kläui, W. *Helv. Chim. Acta* **1977**, *60*, 326. (b) Werner, H.; Feser, R.; Buchner, W. *Chem. Ber.* **1979**, *112*, 834.
(22) (a) Green, M. L. H.; Wong, L. *J. Chem. Soc., Chem. Commun.* **1988**, 677. (b) Bercaw, J. E.; Burger, B. J.; Green, M. L. H.; Santarsiero, B. D.; Sella, A.; Trimmer, M. S.; Wong, L. *J. Chem. Soc., Chem. Commun.* **1989**, 734. (c) Casey, C. P.; Yi, C. S. *Organometallics* **1991**, *10*, 33.

(23) Error limits are based on temperature differences of ±0.5 °C and variations in rate constants of ±10%. In the slowest exchange regions (k <2 s^{-1}), errors in k are considerably greater, ca. ±50%.

Table II. Rate Constants[a] and Free Energies of Activation[b] for Dynamic Processes I and II

compd	k_I (T, °C)	ΔG^*_I[c]	k_{II} (T, °C)	ΔG^*_{II}[d]
3a	6.6 (−84)	10.2	11 (−44)	12.2
3b	47 (−49)	11.3	8.4 (−49)	12.1
4a	168 (−109)	7.8	1.9 (−10)	15.0
4b	431 (−80)	8.8	0.4 (−23)	15.0

[a] Values in s^{-1}. [b] Values in kcal/mol; error limits ca. 0.1 kcal/mol for H migration and ethylene rotation. [c] Determined from line-shape analysis. [d] Determined from line-shape analysis and (or) spin saturation experiments.

complexes. These trends suggest that the greater the electron density at Rh, the higher the rotational barrier. However, in view of the difference in both electronic and steric factors in **3** and **4** and the unknown orientation of ethylene in the transition states for rotation, we have not attempted a detailed analysis of these differences.

The barriers to hydride migration are sensitive to Cp vs Cp* ligand substitution, increasing by ca. 3 kcal/mol in substituting Cp for Cp* in both the PMe_3 and $P(OMe)_3$ cases. The barriers are unaffected by the nature of the phosphine ligand (PMe_3 versus $P(OMe)_3$) in both the Cp and Cp* series. Similar trends are observed in the cobalt analogs[11c] where the barrier to exchange of $H_{agostic}$ with H_1 and H_2 (eq 3) is higher by ca. 1.5 kcal/mol for the Cp systems relative to their Cp* analogs. Like the Rh systems, the barrier is insensitive to PMe_3 relative to $P(OMe)_3$ substitution in the Co analogs.

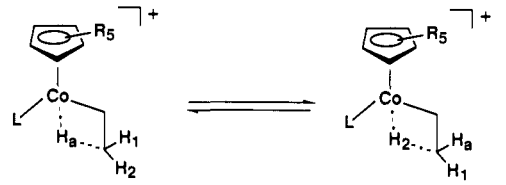

(3)

Two slightly different mechanisms can be considered to account for the three-hydrogen scrambling process. Conceptually simplest is the "classical" migratory insertion mechanism (eq 4) in which a 16-electron ethyl species **6** is formed wherein CH_3 rotation equilibrates the three hydrogens. The transition state **5** would likely be close in energy to the 16-electron species **6** (see below for further support). The second mechanism involves an in-place rotation mechanism[22] which can be depicted as in eq 5. The metal-bound hydrogen begins to bridge C_β and, rather than formation of the 16-electron **6**, exchange is accomplished by in-place rotation. A transition state such as **5'** may be envisioned for this concerted process in which the β-hydrogen(s) never loses contact with the Rh center.

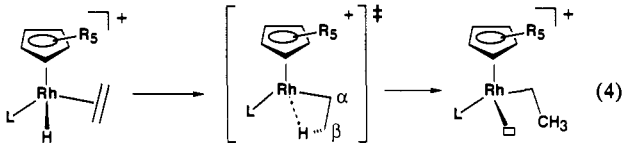

(4)

5 **6**

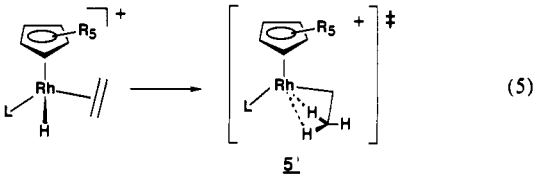

(5)

5'

Our data cannot distinguish between these mechanisms. However, in either case we believe the transition state for β-migratory insertion (**5** or **5'**) must involve a very weak Rh···HC interaction(s) and lie close in energy to the 16-electron species **6**. Support for this assertion comes from the observation that in the closely related cobalt complexes $Cp^*(L)CoCH_2CH_2\text{-}\mu\text{-}H^+$ (L = PMe_3 or PMe_2Ph) the 3-H scrambling barrier is only ca. 2.5 kcal/mol less than that required for inversion at the cobalt center.[11c,13b] The inversion process must proceed through a species involving a 16-electron cobalt ethyl complex with σ_v symmetry and thus no Co···HC_β interaction.

Table III. Selected ^1H and ^{13}C NMR Data for **7** and **8**

compd[a] (T, °C)	δH_1 or δH_2	δH_1 or δH_2	δC_α	δC_β	$J_{C_\alpha Rh}$, Hz	$J_{C_\alpha P}$, Hz
7a (−100)	obscured	obscured	16.2	18.9	10	15
7b (−100)	obscured	obscured	14.8	18.5	8	21
8a (23)	2.32	2.17	11.9	23.7	9	9
8b (23)	2.07	1.46	11.8	24.2	7	13

[a] All spectra were recorded in CD_2Cl_2. Chemical shifts are in ppm relative to TMS taken as 0 ppm.

A plausible explanation for the decrease in the barrier which occurs when substituting Cp* for Cp and the insensitivity of the barrier to PMe_3 relative to $P(OMe)_3$ substitution can be advanced on the basis of the stereochemistry of these ligands relative to the developing empty orbital in the transition state (**5** or **5'**). The σ-donor properties of the ligand trans to the developing empty orbital in the transition state would be expected to exert a greater influence than the cis ligand on the relative transition-state energies. Thus, the better donor trans Cp* ligand lowers the hydride migration barrier relative to Cp, whereas the barrier is insensitive to the substitution of PMe_3 for $P(OMe)_3$ in the cis position.

B. Generation and Spectral Characterization of $C_5R_5(L)Rh(Et)(C_2H_4)^+$ (R = H, Me; L = $P(OMe)_3$, PMe_3) 7 and 8. Observation of the β-Migratory Insertion Reaction. 1. Generation and Spectroscopic Analysis of $C_5R_5(L)Rh(Et)(C_2H_4)^+$ 7 and 8. Treatment of $C_5R_5(L)Rh(H)(C_2H_4)^+$ **3** and **4** with an excess of ethylene results in trapping of the 16-electron species **6** with ethylene to yield the 18-electron ethyl ethylene complexes **7** and **8**. A similar reaction to form **8b** has been reported by Werner.[6b]

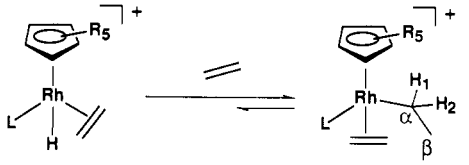

3 R= Me **7** R= Me

4 R= H **8** R= H

L= (a) $P(OMe)_3$ (b) PMe_3

^1H and ^{13}C NMR spectra of these species were recorded, and key parameters are summarized in Table III. Complete spectroscopic data are given in the Experimental Section. In the ^1H NMR spectrum, evidence for the ethyl ethylene complex comes from the observation of a methyl group (triplet) and diastereotopic methylenic protons on C_α due to the chirality at the rhodium center. In the ^{13}C NMR spectrum, substantial Rh–C_α coupling constants (ca. 7–10 Hz) are consistent with Rh–C_α σ bonds. One additional point concerning these systems should be noted: the ethyl ethylene complexes are in equilibrium with the hydride ethylene complexes, and a deficiency of ethylene drives the equilibrium back to the ethylene hydride species. The ratio of **8a**:**4a** was measured by integrating the resonances of C_5H_5 in the ^1H NMR for the two species at 23 °C under 1 atm of ethylene and was found to be ca. 25:1.

2. Mechanism of Dimerization and Rates of β-Migratory Insertion in Ethyl Ethylene Complexes. The ethyl ethylene species described above serve as catalysts for the dimerization of ethylene to butenes. The proposed mechanism is shown in Scheme I. Migratory insertion of **7** and **8** generates the unsaturated rhodium–butyl complex **9** which, upon β-H elimination, must give initially the 1-butene complex **10**. The 2-butene isomers **10'** and **10''** must arise by the well-established mechanism of migratory insertion of **10** to give the Rh–*sec*-butyl complex followed by reelimination. Whether equilibrium is established among isomers **10**–**10''** prior to butene displacement by ethylene is unknown.[24]

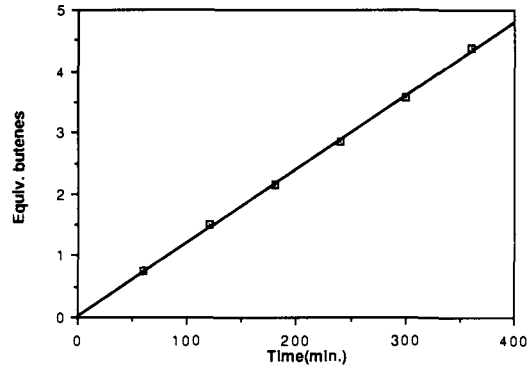

Figure 3. Equivalents of butenes formed versus time at 23 °C for $Cp^*RhP(OMe)_3(C_2H_5)(C_2H_4)^+$ (**7a**).

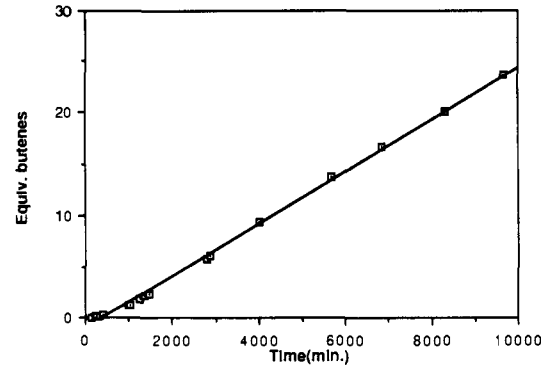

Figure 4. Equivalents of butenes formed versus time at 23 °C for $CpRhP(OMe)_3(C_2H_5)(C_2H_4)^+$ (**8a**).

Scheme I

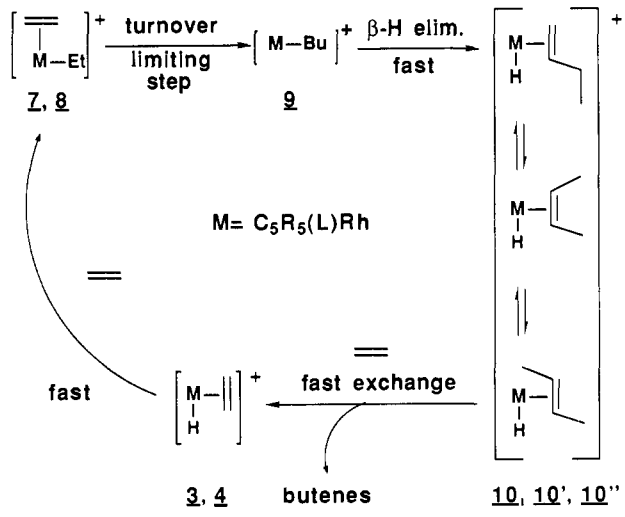

7, 8 9 10, 10', 10'' 3, 4

Following this ethylene dimerization by ^1H NMR at ambient temperature (23 °C) is very informative; since no species other than **7** and **8** can be detected in significant quantities, the turnover-limiting step must be the migratory insertion reaction, **7,8** → **9**. The ethyl ethylene complex is the "resting state" of the catalyst. The rate of ethyl migration, being the turnover-limiting step in the catalytic cycle (see Scheme I), was calculated by monitoring the production of butenes versus time. Both GC and NMR techniques were used, and details of the kinetic runs can be found in the Experimental Section. The free energies of activation for this process fall in the range 22–25 kcal/mol. Typical linear plots of equivalents of butenes formed vs time at 23 °C for **7a** and **8a** are shown in Figures 3 and 4, which yield $k = 2.0 \times 10^{-4}$ s^{-1}, $\Delta G^\ddagger = 22.4$ kcal/mol and $k = 4.7 \times 10^{-5}$ s^{-1}, $\Delta G^\ddagger = 23.4$ kcal/mol, respectively (the complete set of $\Delta G^\ddagger$ values is reported in Table IV in the section comparing the migratory aptitudes of H and Et).[25]

3. Fate of the Catalyst. While our main objective was to measure the rates of migratory insertion reactions of the ethyl ethylene complexes, we wished to know the fate of the catalyst after conversion of the available ethylene to butenes. Would the Rh species remaining affect butene dimerization or would an inactive complex be formed? A brief study was carried out with

Table IV. Free Energies of Activation[a] for Ethyl and Hydride Migration for $C_5R_5Rh(L)(C_2H_4)R^+$

compd	$\Delta G^\ddagger_{\text{Et mig}}$[b]	$\Delta G^\ddagger_{\text{H mig}}$	$\Delta\Delta G^\ddagger_{\text{(Et-H)mig}}$
3,7 (a)	22.4	12.2	10.2
3,7 (b)	23.4	12.1	11.3
4,8 (a)	23.4	15.0	8.4
4,8 (b)	24.7	15.0	9.7

[a] Values in kcal/mol; error limits ca. 0.1 kcal/mol for H migration and ca. ±0.2 kcal/mol for Et migration. [b] Determined from the rate of production of butenes at 23 °C by GC or NMR techniques.

the $CpRhP(OMe)_3(C_2H_4)H^+$ system. In order to reproduce the conditions at the end of the catalysis where the ethylene has been completely consumed, the hydride complex $CpRhP(OMe)_3(C_2H_4)H^+$ (**4a**) was exposed to a large excess of 1-butene. Rapid catalytic equilibration of 1-butene with *trans*(major)- and *cis*-(minor)-2-butenes is initially observed. The high-field region reveals numerous isomeric butene hydride species $CpRhP(OMe)_3(C_4H_8)H^+$, whose detailed structures could not be assigned (δ −9.14, dd, $J_{PH} = 22$ Hz, $J_{RhH} = 14$ Hz; −9.44, t, $J = 14$ Hz; −10.24, t, $J = 15$ Hz; −11.35 broad; −12.82, t, $J = 16$ Hz). After standing at 25 °C for 3 days, a new species appears (δCp = 5.68 ppm) which accounts for ca. 50% of the rhodium complexes. After 6 days this species is the major complex (>85%); a methyl doublet at 1.85 ppm ($^3J_{HH} = 6$ Hz) and a one-proton signal at 5.24 ppm (dt, $^3J_{cis} = 7$ Hz, $^3J_{trans} = 11$ Hz) strongly suggested that this new species was a *syn*-1-methallyl complex. Complete ^1H and ^{13}C NMR spectra of this species isolated free of the minor butene hydride complexes confirmed the methallyl structure (see the Experimental Section for details). A minor isomer also possessing syn stereochemistry could be detected, as evidenced by a methyl doublet at 1.8 ppm ($^3J_{HH} = 6$ Hz) and a doublet of triplets ($^3J_{cis} = 6$ Hz, $^3J_{trans} = 11$ Hz) at 4.94 ppm. Single crystals of the major isomer were isolated from CD_2Cl_2, and X-ray analysis confirmed the syn geometry and established the structure as the cisoid, syn isomer **11**. The minor isomer is assumed to be the transoid, syn isomer **12**. Similar allylic systems, $CpRh(^iPr_3P)(\eta^3\text{-crotyl})^+$, prepared by a different route have been described by Werner in 1987[26] and Stryker[27] in 1992. The formation of these allylic species is relevant to Rh(III)-catalyzed dimerization of olefins since we recently demonstrated that formation of an allylic species derived from a similar Rh system used for the dimerization of methyl acrylate was responsible for the short lifetime of the catalyst.[28]

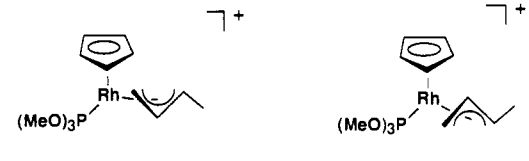

11 12

(24) Little information can be derived from the ratio of butene isomers formed in these reactions since (1) the ratios of **10**, **10'**, and **10''** during catalysis are unknown as are the rates of butene displacement from each isomer, and (2) isomer ratios can vary with time due to isomerization of butenes after formation. We observe isomerization of butenes to their thermodynamic ratios at the end of catalysis when all of the ethylene is consumed.

(25) Preliminary results suggest that the methyl migration barriers in the analogous methyl ethylene complexes $CpRh(L)(C_2H_4)(CH_3)^+$ are ca. 1 kcal/mol higher than their ethyl ethylene counterparts; however, the propene hydride complexes are not cleanly formed under the conditions required for methyl migration. This difference likely reflects the difference in bond energies between Rh–CH_3 and Rh–CH_2–CH_3.

(26) Werner, H.; Wolf, J. *Organometallics* **1987**, *6*, 1164.
(27) Stryker, J. M.; Tjaden, E. B. *Organometallics* **1992**, *11*, 16.
(28) (a) Brookhart, M.; Sabo-Etienne, S. *J. Am. Chem. Soc.* **1991**, *113*, 2777. (b) Brookhart, M.; Hauptman, E. *J. Am. Chem. Soc.* **1992**, *114*, 4437.

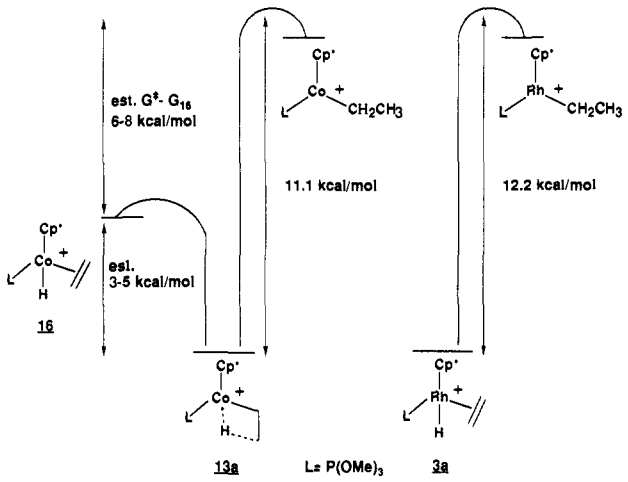

Figure 5. Free energy diagrams illustrating the dynamic behavior of the cobalt and rhodium hydride complexes **13a** and **3a**.

C. Comparison of H vs R Migratory Insertion. The free energies of activation for the β-migratory insertion reactions of the series of rhodium ethylene hydride and ethylene ethyl complexes are summarized in Table IV. This is the first such series where barriers for β-hydride migration have been compared directly with the analogous barriers for β-alkyl migration. The barriers to ethyl migration relative to those for hydride migration show a parallel but somewhat diminished sensitivity to Cp versus Cp* substitution. The hydride barriers increase by ca. 3 kcal/mol in substituting Cp for Cp*, while the corresponding barriers to ethyl migration increase only by ca. 1 kcal/mol. The hydride barriers are insensitive to $P(OMe)_3$ versus PMe_3 substitution, while the ethyl migration barriers increase ca. 1 kcal/mol upon replacing $P(OMe)_3$ by PMe_3. The origins of these small differences are not apparent. In considering the diminished sensitivity to Cp versus Cp* substitution in the ethyl complexes, it seems possible that the transition state for alkyl migration still involves substantial $Rh\text{–}C_\alpha$ interaction and thus shows less unsaturated character than the transition state for hydride migration (see above). Such a transition-state difference would translate into less sensitivity to the σ-donor properties of the trans ligands (Cp and Cp*) consistent with observations.

A significant point here is that in this series of similar complexes the differences in free energies of activation, $\Delta\Delta G^{\ddagger}$'s, for H versus CH_2CH_3 groups lie in the range of 8.5–11 kcal/mol. The hydride migration barriers can be accurately extrapolated to 23 °C, the temperature at which the ethyl migration barriers were measured. Thus, as 23 °C the $\Delta\Delta G^{\ddagger}$ values correspond to relative migratory insertion rates k_H/k_{Et} of 10^6–10^8.

It is instructive to compare these rates and barriers to other organometallic systems where such estimates can be made. Bercaw[2b] has reported that the $\Delta G^{\ddagger}$ for α-H migratory insertion in $Cp^*_2Ta(=CH_2)(H)$ is 16.2 kcal/mol, while the corresponding value for α-CH_3 migration in $Cp^*_2Ta(=CH_2)(CH_3)$ is 30.3 kcal/mol, yielding $\Delta\Delta G^{\ddagger}$ = 14 kcal/mol. The β-H migration rate obtained for the $Cp^*_2Ta(C_2H_4)(H)$ complex was 20.8 kcal/mol. The β-CH_3 migratory insertion of $Cp^*_2Ta(C_2H_4)(CH_3)$ has not been observed even at elevated temperatures. As noted by Bercaw, this is not surprising since $\Delta G^{\ddagger}$ for this process would be expected to fall in the 30–35 kcal/mol range on the basis of the $\Delta\Delta G^{\ddagger}$ value for the $Cp^*_2Ta(=CH_2)(R)$ (R = H, CH_3) system as well as the $\Delta\Delta G^{\ddagger}$ values reported here for the Rh systems.

Cooper[4] has reported the activation energy for migratory insertion in the endo isomer of $Cp_2W(CH_2{=}CHCH_3)(H)^+$ as 24 kcal/mol. The migratory insertion process in the known alkyl analog $Cp_2W(C_2H_4)(CH_3)^+$ has not been effected.[15] Again, this must be due to a very high free energy of activation (greater than ca. 35 kcal/mol) as predicted on the basis of the hydride barrier.

Werner[6a] has reported both $(C_6H_6)(PMe_3)Ru(H)(C_2H_4)^+$ and $(C_6H_6)(PMe_3)Ru(CH_3)(C_2H_4)^+$, but a detailed kinetic analysis was not described for the migratory insertion of the hydride complex. From the description of the dynamic NMR spectrum of $(C_6H_6)(PMe_3)Ru(H)(C_2H_4)^+$, the rate of H migration must be similar to that observed for **3** and **4**. No methyl migration was reported for $(C_6H_6)(PMe_3)Ru(CH_3)(C_2H_4)^+$, but on the basis of our results the free energy of activation for such a process should be in a range feasible for observation.

Comparison of the energetics of the rhodium systems studied here with the corresponding cobalt systems **13** and **14** is most informative. While free energies of activation for site exchange of H_a with the β-hydrogens for all four complexes (**13a,b** and **14a,b**) have been reported,[11c] the barrier for migratory insertion in the ethyl ethylene analogs is known only for **15a**.[18] Thus, comparisons will be restricted to the $Cp^*/P(OMe)_3$ systems.

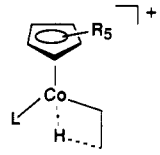

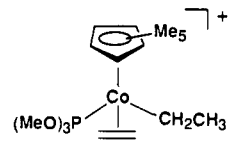

13 R= Me

14 R= H

15a

L= (a) $P(OMe)_3$ (b) PMe_3

The barrier to migratory insertion for **15a** of 14.3 kcal/mol is less than that for the second-row rhodium analog **7a**, 22.4 kcal/mol. A similar effect has been noted by Bercaw in comparing the second-row niobium complexes $(C_5R_5)_2Nb(C_2H_4)H$ (R = H, Me) with the third-row tantalum analog $(C_5R_5)_2Ta(C_2H_4)H$ (R = H, Me), but the magnitude of the difference (ca. 3 kcal/mol) is substantially less.[2c]

At first glance, the barriers to hydride migration in $Cp^*Rh\text{-}P(OMe)_3(C_2H_4)H^+$ (12.2 kcal/mol) and $Cp^*P(OMe)_3\text{-}CoCH_2CH_2\text{-}\mu\text{-}H^+$ (11.1 kcal/mol) appear unexpectedly close. However, the stable form of the cobalt hydride **13a** is agostic not terminal. To properly compare the Rh and Co systems, the energy difference between the terminal cobalt hydride **16** and the transition state for hydride migration must be used. We have been able to estimate the energy difference between the agostic complex **13a** and terminal hydride **16** as 3–5 kcal/mol.[29] Thus, the free energy difference, $G^{\ddagger}_{Hmig.} - G_{16}$, can be estimated as 6–8 kcal/mol, which is significantly less than the corresponding 12.2 kcal/mol difference in the Rh system as expected. These relationships are illustrated in the free energy diagrams shown in Figure 5, which compare the agostic cobalt system with the rhodium system.

The $\Delta\Delta G^{\ddagger}$ value of ca. 6–8 kcal/mol is less for the first-row cobalt system than the $\Delta\Delta G^{\ddagger}$ value of 10.2 kcal/mol for the rhodium system, consistent with the expectation that as the barriers decrease the difference between the barriers will decrease. The quantitative comparison provided by the Co and Rh analogs lends support for the suggestion that barriers to β-migratory insertion in alkyl–olefin complexes will be, in general, lower for cases in which the hydride analogs exist as agostic rather than terminal hydrides.

Experimental Section

General Information. All complexes were manipulated under an atmosphere of dry, oxygen-free nitrogen within a Vacuum Atmospheres dry box or on a standard Schlenk line. Methylene chloride was distilled in an N_2 atmosphere from phosphorus pentaoxide prior to use. Tetrahydrofuran, toluene, and hexane were distilled in an N_2 atmosphere from sodium and benzophenone prior to use. Methanol was distilled from $Mg(OMe)_2$ prior to use. Solvents for column chromatography were degassed by purging with nitrogen gas for 10 min. ^1H and ^{13}C NMR spectra were recorded on either a Varian XL-400, Bruker WM-200, or Bruker WM-250 spectrometer. Chemical shifts were reported by reference to protonated residues of solvents. Ethylene was purified by passage over an oxygen-scavenging copper catalyst (BASF catalyst R 3-11) and water-scavenging molecular sieves (4 Å). Elemental analyses

(29) Brookhart, M.; Lincoln, D. M.; Bennett, M.; Pelling, S. *J. Am. Chem. Soc.* **1990**, *112*, 2691.

were performed by Oneida Research Services, Inc. Gas chromatography (GC) analyses were conducted on a Hewlett-Packard 5750 using flame ionization detection and a 50-m capillary fused silica column with Al_2O_3/KCl as the active phase. The following preparations were based on standard literature procedures: $[Rh(C_2H_4)_2Cl]_2$[30] and $CpRh(C_2H_4)_2$.[31]

$Cp^*RhP(OMe)_3(C_2H_4)$ (1a). The following procedure was modeled after one reported by Jones.[32] In a typical reaction, 250 mg (0.85 mmol) of $C_5Me_5Rh(C_2H_4)_2$ was weighed in a dry box and dissolved in 30 mL of dry, degassed toluene in a Schlenk flask under nitrogen. Trimethyl phosphite (66 μL, 0.93 mmol) was added to the yellow toluene solution. A condenser with a nitrogen purge was fitted to the Schlenk flask. The entire system was kept under nitrogen, and the solution was refluxed for 4 h over which time it turned from yellow to orange-yellow. The solution was then cooled to 25 °C and filtered through Celite. The toluene was removed under vacuum. The remaining yellow-orange solid was dissolved in 25 mL of 2-methylbutane, filtered through Celite, and slowly cooled to −78 °C to yield 232–265 mg (70–80% yield) of the product as yellow-orange crystals. Crystals were air-sensitive and thermally stable: ^1H NMR (400 MHz, C_6D_6, 23 °C) δ 1.85 (d, J_{PH} or J_{RhH} = 3 Hz, $C_5(CH_3)_5$), 3.28 (d, J_{PH} = 12 Hz, $P(OCH_3)_3$), 2.20, 1.67 (m, C_2H_4); ^{13}C NMR (100 MHz, C_6D_6, 23 °C) δ 96.3 (dd, $J_{RhC} = J_{PC}$ = 4 Hz, $C_5(CH_3)_5$), 49.8 (q, J_{CH} = 145 Hz, $P(OCH_3)_3$), 34.4 (ddt, J_{RhC} = 14 Hz, J_{PC} = 4 Hz, J_{CH} = 150 Hz, C_2H_4), 10.2 (q, J_{CH} = 126 Hz, $C_5(CH_3)_5$). Anal. Found (Calcd): C, 45.94 (46.16); H, 6.99 (7.23).

$Cp^*RhPMe_3(C_2H_4)$ (1b). This compound was prepared according to the procedure reported by Jones.[32] For comparison purposes, complete NMR data of this compound follows: ^1H NMR (400 MHz, C_6D_6, 23 °C) δ 1.90 (d, J_{PH} or J_{RhH} = 2 Hz, $C_5(CH_3)_5$), 1.62, 1.72 (m, C_2H_4), 0.85 (dd, J_{PH} = 13 Hz, J_{RhH} = 2 Hz, $P(CH_3)_3$); ^{13}C NMR (100 MHz, C_6D_6, 23 °C) δ 95.1 (d, J_{RhC} = 4 Hz, $C_5(CH_3)_5$), 31.1 (dt, J_{RhC} or J_{PC} = 16 Hz, J_{CH} = 153 Hz, C_2H_4), 16.9 (dq, J_{PC} = 25 Hz, J_{CH} = 127 Hz, $P(CH_3)_3$), 10.6 (q, J_{CH} = 126 Hz, $C_5(CH_3)_5$).

$CpRhP(OMe)_3(C_2H_4)$ (2a). Trimethyl phosphite (93 μL, 0.79 mmol) was added to $CpRh(C_2H_4)_2$ (160 mg, 0.7 mmol) in 20 mL of toluene. The mixture was heated for 3 h under reflux. The ^1H NMR spectrum of the crude material showed the ratios of the bis-ethylene to the monophosphite to the bisphosphite to be 32:54:14. The solvent was then removed under vacuum, and 10 mL of hexane was added to the dark orange residue. The crude material was separated by chromatography on a column of alumina. The first yellow band, containing $CpRh(C_2H_4)_2$, was eluted with hexane, and the second, containing the product $CpRhP(OMe)_3(C_2H_4)$ (**2a**), was eluted with 5:1 hexane/methylene chloride. Recrystallization of **2a** from hexane at −78 °C forms brown crystals which melt to an oil at room temperature: ^1H NMR (400 MHz, CD_2Cl_2, 23 °C) δ 5.25 (d, J_{RhH} or J_{PH} = 2 Hz, C_5H_5), 3.48 (d, J_{RhH} = 12 Hz, $P(OCH_3)_3$), 1.62, 2.5 (m, C_2H_4); ^{13}C NMR (100 MHz, CD_2Cl_2, 23 °C) δ 86.1 (ddd, $J_{CP} = J_{CRh}$ = 4 Hz, J_{CH} = 179 Hz, C_5H_5), 51.2 (q, J_{CH} = 145 Hz, $P(OCH_3)_3$), 26.2 (ddt, J_{CRh} = 14 Hz, J_{CP} = 4 Hz, J_{CH} = 156 Hz, C_2H_4). Anal. Found (Calcd): C, 37.52 (37.52); H, 5.69 (5.67).

$CpRhPMe_3(C_2H_4)$ (2b). This compound was prepared according to the procedure reported by Werner.[33] For comparison purposes, complete NMR data of this compound follow: ^1H NMR (400 MHz, C_6D_6, 23 °C) δ 5.12 (s, C_5H_5), 2.78, 1.49 (m, C_2H_4), 0.79 (dd, J_{PH} = 9 Hz, J_{RhH} = 1 Hz, $P(CH_3)_3$); ^{13}C NMR (100 MHz, C_6D_6, 23 °C) δ 85.4 (d, J_{CH} = 173 Hz, C_5H_5), 23.7 (dt, J_{RhC} = 16 Hz, J_{CH} = 153 Hz, C_2H_4), 19.7 (dq, J_{PC} = 28 Hz, J_{CH} = 128 Hz, $P(CH_3)_3$).

$[Cp^*RhP(OMe)_3(C_2H_4)H^+][BF_4^-]$ (3a). $Cp^*RhP(OMe)_3(C_2H_4)$ (10 mg, 0.0256 mmol) was weighed in a dry box and dissolved in 0.4 mL of CD_2Cl_2 in an NMR tube. The solution was cooled to −30 °C. To this solution was added $HBF_4{\cdot}Me_2O$ (1.3 equiv) dissolved in 0.4 mL of CD_2Cl_2. The solution was allowed to warm to approximately 0 °C while stirring. Once the acid had completely dissolved, the yellow solution was frozen in liquid nitrogen and sealed under vacuum. The sample was warmed to −80 °C and introduced into a −80 °C precooled NMR probe. ^{13}C NMR samples were prepared in a similar fashion employing 30 mg (0.256 mmol) of the neutral precursor and 1.3 equiv of $HBF_4{\cdot}Me_2O$. An alternative procedure was used when excess acid was not desired in the sample. $Cp^*RhP(OMe)_3(C_2H_4)$ (25 mg, 0.064 mmol) was weighed in the dry box and transferred to a Schlenk tube. The solid was dissolved in 10–15 mL of diethyl ether under N_2. The solution was cooled to −30 °C, and 1.3 equiv of $HBF_4{\cdot}Me_2O$ in 5 mL of diethyl ether was added via syringe. The cationic hydride complex rapidly precipitated from solution. The solution was cooled to −80 °C. The ether solution was removed via cannula, and the solid was washed with two 5-mL portions of cold diethyl ether. The solid was dried under vacuum at −30 °C. Warming the solid to higher temperatures resulted in decomposition; thus, elemental analysis was not possible. The complex was dissolved in 0.8 mL of CD_2Cl_2 and transferred via cannula to an NMR tube. The sample was frozen and sealed under vacuum. **3a**: ^1H NMR (400 MHz, CD_2Cl_2, −94 °C) δ 3.51 (d, J_{PH} = 13 Hz, $P(OCH_3)_3$), 3.0, 2.9, 2.6, 2.5 (m, C_2H_4), 1.85 (d, J_{PH} or J_{RhH} = 4 Hz, $C_5(CH_3)_5$), −9.95 (dd, $J_{PH} = J_{RhH}$ = 18 Hz, H); ^{13}C NMR (100 MHz, CD_2Cl_2, −94 °C) δ 104.4 (s, $C_5(CH_3)_5$), 52.7 (dq, J_{PC} = 3 Hz, J_{CH} = 149 Hz, $P(OCH_3)_3$), 10.0 (q, J_{CH} = 129 Hz, $C_5(CH_3)_5$); ethylene signals are obscured by solvent but are visible in acetone-d_6 at −94 °C δ 53.4 (t, J_{CH} = 161 Hz, C_α or C_β), 54.6 (t, J_{CH} = 161 Hz, C_α or C_β).

$[Cp^*RhPMe_3(C_2H_4)H^+][BF_4^-]$ (3b). Samples of **3b** were prepared as for **3a** using $Cp^*RhPMe_3(C_2H_4)$ as the neutral precursor. Attempts to isolate **3b** as a stable salt at 23 °C were unsuccessful: ^1H NMR (400 MHz, CD_2Cl_2, −80 °C) δ 2.93, 2.53, 2.42, 2.27 (m, C_2H_4), 1.85 (s, $C_5(CH_3)_5$), 1.32 (d, J_{PH} = 11 Hz, $P(CH_3)_3$), −10.7 (dd, J_{PH} or J_{RhH} = 18 Hz, J_{PH} or J_{RhH} = 31 Hz, H); ^{13}C NMR (100 MHz, CD_2Cl_2, −80 °C) δ 102.9 (dd, $J_{PC} = J_{RhC}$ = 4 Hz, $C_5(CH_3)_5$), 51.7 (dt, J_{PC} or J_{RhC} = 9 Hz, J_{CH} = 164 Hz, C_α or C_β), 49.2 (dt, J_{PC} or J_{RhC} = 9 Hz, J_{CH} = 163 Hz, C_α or C_β), 15.9 (dq, J_{PC} = 36 Hz, J_{CH} = 130 Hz, $P(CH_3)_3$), 9.8 (q, J_{CH} = 128 Hz, $C_5(CH_3)_5$).

$[CpRhP(OMe)_3(C_2H_4)H^+][BF_4^-]$ (4a). $CpRhP(OMe)_3(C_2H_4)$ (10 mg, 0.031 mmol) was weighed under nitrogen and dissolved in 0.6 mL of CD_2Cl_2 in an NMR tube blanketed with nitrogen and equipped with a side arm. The solution was frozen in liquid nitrogen on a standard vacuum line. $HBF_4{\cdot}Me_2O$ complex (1.3 equiv, 0.041 mmol) was syringed into the NMR tube. The tube was frozen and sealed under vacuum. The sample was progressively warmed until the $HBF_4{\cdot}Me_2O$ complex completely dissolved and formed a clear orange solution (ca. −30 °C); the sample was then introduced into a precooled probe for analysis. ^{13}C NMR samples were prepared in a similar fashion employing 70 mg of the neutral precursor and 1.3 equiv of $HBF_4{\cdot}Me_2O$. Repeated attempts to isolate this species as a stable salt at 23 °C were not successful: ^1H NMR (CD_2Cl_2, 250 MHz, −20 °C) δ 5.80 (d, J_{RhH} = 2 Hz, C_5H_5), 3.64 (d, J_{PH} = 13 Hz, $P(OMe)_3$), 3.17, 3.52 (m, C_2H_4), −9.94 (dd, J_{RhH} = 15 Hz, H); ^{13}C NMR (CD_2Cl_2, 62 MHz, 23 °C) δ 92.5 (ddd, $J_{RhC} = J_{PC}$ = 3 Hz, J_{CH} = 179 Hz, C_5H_5), 54.3 (dq, J_{PC} = 6 Hz, J_{CH} = 159 Hz, $P(OCH_3)_3$), 47.9 (dt, J_{RhC} = 9 Hz, J_{CH} = 157 Hz, C_2H_4). At −114 °C, the ethylenic carbons are static and appear as two signals at 48.3 and 47.1 ppm.

$[CpRhPMe_3(C_2H_4)H^+][BF_4^-]$ (4b). This compound has been reported by Werner.[33] The following synthesis is a modified version of Werner's synthesis and is analogous to the synthesis used for the $C_5(CH_3)_5$ derivatives. $CpRhPMe_3(C_2H_4)$ (130 mg, 0.48 mmol) was weighed in the dry box and transferred to a Schlenk flask. The solid was dissolved in 5 mL of diethyl ether under N_2. The solution was cooled to −30 °C, and 69 μL (1.3 equiv, 0.62 mmol) of $HBF_4{\cdot}Me_2O$ in 15 mL of diethyl ether was added via syringe. The cationic hydride complex rapidly precipitated from solution. The ether solution was removed via cannula, and the solid was washed twice with 5 mL of cold diethyl ether. The solid was dried under vacuum at −30 °C. The resulting pinkish solid is formed in 80% yield (137 mg, 0.38 mmol): ^1H NMR (CD_2Cl_2, 400 MHz, −20 °C) δ 5.72 (d, J_{RhH} or J_{PH} = 1 Hz, C_5H_5), 3.49, 2.92 (m, C_2H_4), 1.57 (dd, J_{PH} = 12 Hz, J_{RhH} = 1 Hz, $P(CH_3)_3$), −10.66 (broad, H); ^{13}C NMR (100 MHz, CD_2Cl_2, 20 °C) δ 92.6 (ddd, $J_{RhC} = J_{PC}$ = 4 Hz, J_{CH} = 179 Hz, C_5H_5), 45.0 (dt, J_{RhC} = 9 Hz, J_{CH} = 159 Hz, C_2H_4), 20.2 (dq, J_{PC} = 38 Hz, J_{CH} = 131 Hz, $P(CH_3)_3$). At −92 °C, the ethylenic carbons are static and appear as two signals at 46.0 and 47.0 ppm.

Dynamic Analysis of 3 and 4 Using NMR Techniques. ^1H and ^{13}C NMR samples were prepared as described above for each complex.

A. Kinetics of Hydride Migration. 1. Magnetization Transfer Experiments. Prior to performing the spin saturation transfer experiments, the relaxation times T_1 for the ethylenic protons and the hydride were measured for each temperature using the inversion recovery method and analyzed with the spectrometer T_1 routine. The hydride signal was then saturated, and the decrease in intensity of the olefinic resonances was measured. After carrying out the standard spin saturation transfer analysis, the rate was calculated using the equation $k = (1/T_1)(M(0)/M(\infty) - 1)$, where $M(0)$ and $M(\infty)$ are the intensities of the olefinic resonances before and after spin saturation, respectively. $Cp^*RhP(OMe)_3(C_2H_4)H^+$ (**3a**): $k(-39\ °C) = 28\ s^{-1}$, $\Delta G^\ddagger = 12.0$ kcal/mol. $Cp^*RhPMe_3(C_2H_4)H^+$ (**3b**): $k(-49\ °C) = 35\ s^{-1}$, $\Delta G^\ddagger = 11.4$ kcal/mol. $CpRhP(OMe)_3(C_2H_4)H^+$ (**4a**): $k(-10\ °C) = 3.5\ s^{-1}$, $\Delta G^\ddagger = 14.7$ kcal/mol. $CpRhPMe_3(C_2H_4)H^+$ (**4b**): $k(-23\ °C) = 0.4\ s^{-1}$, $\Delta G^\ddagger = 15.0$ kcal/mol.

2. Line Broadening Experiments. The line broadening experiments were carried out for **4** beginning at a temperature where the complexes were static (the hydrides appeared as a sharp doublet of doublets) and

(30) Cramer, R. *Inorg. Synth.* **1974**, *15*, 14.
(31) King, R. B. *Inorg. Chem.* **1963**, *2*, 528.
(32) Jones, W. D.; Feher, F. J. *Inorg. Chem.* **1984**, *23*, 2376.
(33) Werner, H.; Feser, R. *J. Organomet. Chem.* **1982**, *232*, 351.

continuing to a temperature where the complexes were dynamic (the hydrides appeared as broad signals). Experimental line shapes were compared to line shapes calculated using the DNMR3 program (for an illustration, see Figure 1). This dynamic NMR fitting program gave values of rate constants (k) comparable to those obtained using the slow exchange rate approximation, $k = \pi\Delta\nu$. The DNMR3 rate constants were used to calculate free energies of activation using the Eyring equation. $CpRhP(OMe)_3(C_2H_4)H^+$ (**4a**): $\Delta G^\ddagger$ = 15.0 kcal/mol; k(−20 °C) = 0.6 ± 0.4 s^{-1}; k(−10 °C) = 2.0 ± 0.3 s^{-1}; k(0 °C) = 5.8 ± 0.6 s^{-1}; k(5 °C) = 9.7 ± 1 s^{-1}; k(10 °C) = 16 ± 1.6 s^{-1}; k(20 °C) = 41 ± 4 s^{-1}. $CpRhPMe_3(C_2H_4)H^+$ (**4b**): $\Delta G^\ddagger$ = 14.8 kcal/mol; k(−21 °C) = 0.8 ± 0.5 s^{-1}; k(−10 °C) = 2.9 ± 0.4 s^{-1}; k(−5 °C) = 5 ± 0.5 s^{-1}; k(0 °C) = 8.5 ± 0.9 s^{-1}; k(5 °C) = 14 ± 1.4 s^{-1}; k(10 °C) = 23 ± 2 s^{-1}; k(20 °C) = 58 ± 6 s^{-1}.

B. Kinetics of Ethylene Rotation. Ethylene rotation rates were calculated using either coalescence or slow exchange techniques using broad band decoupled ^{13}C NMR signals. For compounds **3** and **4b** line widths of the two C_2H_4 signals in the slow exchange region can be used to determine the rate of ethylene rotation using the approximation $k = \pi\Delta w$, $\Delta w = w - w_0$, where w_0 is the natural line width. $Cp^*RhP(OMe)_3(C_2H_4)H^+$ (**3a**): k(−84 °C) = 6.6 s^{-1}; $\Delta G^\ddagger$ = 10.2 kcal/mol (^1H NMR spin saturation experiment). $Cp^*RhPMe_3(C_2H_4)H^+$ (**3b**): k(−49 °C) = 47 s^{-1}; $\Delta G^\ddagger$ = 11.3 kcal/mol. $CpRhPMe_3(C_2H_4)H^+$ (**4b**): k(−92 °C) = 60 s^{-1}; $\Delta G^\ddagger$ = 9.0 kcal/mol. Alternatively, for compounds **4** the rates of ethylene rotation at the coalescence temperature were calculated from the frequency separation of the two C_2H_4 signals in the slow exchange limit using the Gutowsky–Holm approximation, $k = \pi(\nu_a - \nu_x)/(2)^{1/2}$. $CpRhP(OMe)_3(C_2H_4)H^+$ (**4a**): k(−109 °C) = 168 s^{-1}; $\Delta G^\ddagger$ = 7.8 kcal/mol. $CpRhPMe_3(C_2H_4)H^+$ (**4b**): k(−80 °C) = 431 s^{-1}; $\Delta G^\ddagger$ = 8.8 kcal/mol.

Generation and Characterization of the Ethyl Ethylene Complexes 7 and 8. The NMR samples were prepared as for **3** and **4** with the following exceptions: 5-mm heavy- or medium-walled NMR tubes were used because of the high ethylene pressures; the amounts of CD_2Cl_2 were only 75% of those used in the preparation of **3** and **4** to allow sufficient headspace for the added ethylene. For complexes **7**, 30–50 equiv of ethylene were condensed into the NMR tube; for complexes **8** ethylene was bubbled into the NMR tube for a few minutes at −10 °C. In either case, once the excess ethylene was introduced, the tube was sealed and the sample characterized at low temperatures.

[$Cp^*RhP(OMe)_3(C_2H_5)(C_2H_4)^+$][$BF_4^-$] (7a): ^1H NMR (400 MHz, CD_2Cl_2, −117 °C) δ 3.75 (d, J_{PH} = 11 Hz, $P(OMe)_3$), 3.45, 2.84, 2.7, 2.43 (m, C_2H_4), 1.69 (d, J_{PH} = 4 Hz, $C_5(CH_3)_5$), 1.17 (dd, J = 7 Hz, CH_3), the missing ^1H CH_2 resonance is probably obscured by the $C_5(CH_3)_5$ resonance; ^{13}C NMR (100 MHz, CD_2Cl_2, −94 °C) δ 104.3 (s, $C_5(CH_3)_5$), 65.0 (br, C_2H_4), 58.5 (br, C_2H_4), 52.7 (dq, J_{PC} = 10 Hz, J_{CH} = 148 Hz, $P(OCH_3)_3$), 18.9 (q, J_{CH} = 127 Hz, CH_2CH_3), 16.2 (ddt, J_{PC} or J_{RhC} = 10 Hz, J_{PC} or J_{RhC} = 15 Hz, J_{CH} = 144 Hz, CH_2CH_3), 8.4 (q, J_{CH} = 129 Hz, $C_5(CH_3)_5$).

[$Cp^*RhPMe_3(C_2H_5)(C_2H_4)^+$][$BF_4^-$] (7b): ^1H NMR (400 MHz, CD_2Cl_2, −100 °C) δ 2.70, 2.70, 2.55, 2.40 (m, C_2H_4), 1.60 (d, J_{RhH} or J_{PH} = 2.5 Hz, $C_5(CH_3)_5$), 1.24 (d, J_{PH} = 11 Hz, PMe_3), 1.20 (dd, J = 9 Hz, CH_3), the missing ^1H CH_2 resonance is probably obscured by the $C_5(CH_3)_5$ resonance; ^{13}C NMR (100 MHz, CD_2Cl_2, −100 °C) δ 103.0 (s, $C_5(CH_3)_5$), 61.0 (dt, J_{PC} or J_{RhC} = 9 Hz, J_{CH} = 146 Hz, C_2H_4), 58.8 (dt, J_{PC} or J_{RhC} = 7 Hz, J_{CH} = 144 Hz, C_2H_4), 18.5 (q, J_{CH} = 128 Hz, CH_2CH_3), 14.8 (ddt, J_{PC} or J_{RhC} = 21 Hz, J_{PC} or J_{RhC} = 8 Hz, J_{CH} = 140 Hz, CH_2CH_3), 8.8 (q, J_{CH} = 140 Hz, $C_5(CH_3)_5$).

[$CpRhP(OMe)_3(C_2H_5)(C_2H_4)^+$][$BF_4^-$] (8a): ^1H NMR (400 MHz, CD_2Cl_2, 23 °C) δ 5.68 (d, J_{RhH} = 3 Hz, C_5H_5), 3.80, 3.30 (m, C_2H_4), 3.70 (d, J_{PH} = 13 Hz, $P(OMe)_3$), 2.32, 2.17 (m, CH_2), 1.44 (dd, J = 8 Hz, CH_3); ^{13}C NMR (100 MHz, CD_2Cl_2, 23 °C) δ 95.5 (ddd, J_{PC} = J_{RhC} = 4 Hz, J_{CH} = 180 Hz, C_5H_5), 58.5 (dt, J_{PC} or J_{RhC} = 6 Hz, J_{PC} or J_{RhC} = 4 Hz, J_{CH} = 165 Hz, C_2H_4), 55.3 (dq, J_{PC} = 8 Hz, J_{CH} = 149 Hz, $P(OCH_3)_3$), 23.7 (q, J_{CH} = 126 Hz, CH_2CH_3), 11.9 (ddt, J_{PC} = J_{RhC} = 9 Hz, J_{CH} = 140 Hz, CH_2CH_3).

[$CpRhPMe_3(C_2H_5)(C_2H_4)^+$][$BF_4^-$] (8b). This compound has been reported by Werner.[6b] For comparison purposes, complete NMR data for this compound follow: ^1H NMR (400 MHz, CD_2Cl_2, 23 °C) δ 5.62 (d, J_{PH} or J_{RhH} = 1 Hz, C_5H_5), 3.47, 3.27 (m, C_2H_4), 2.07, 1.46 (m, CH_2), 1.58 (dd, J_{PH} = 11 Hz, J_{RhH} = 1 Hz, $P(CH_3)_3$), 1.51 (dd, J = 7 Hz, CH_3); ^{13}C NMR (100 MHz, CD_2Cl_2, 23 °C) δ 95.8 (ddd, J_{PC} = J_{RhC} = 4 Hz, J_{CH} = 181 Hz, C_5H_5), 55.9 (dt, J_{PC} or J_{RhC} = 9 Hz, J_{CH} = 166 Hz, C_2H_4), 24.2 (q, J_{CH} = 126 Hz, CH_2CH_3), 17.2 (dq, J_{PC} = 37 Hz, J_{CH} = 113 Hz, $P(CH_3)_3$), 11.8 (ddt, J_{PC} or J_{RhC} = 13 Hz, J_{PC} or J_{RhC} = 7 Hz, J_{CH} = 138 Hz, CH_2CH_3).

Kinetics of Ethyl Migration in Complexes 7 and 8 Using NMR and GC Techniques. A. Dimerization Followed by NMR Spectroscopy. The NMR samples were prepared as for the characterization of **7** and **8**. The tubes were sealed and warmed to ambient temperature (23 °C), and the dimerization reaction was followed by ^1H NMR. The production of butenes (1-butene, *cis*- and *trans*-butenes) was followed versus time and gave a linear plot with a slope corresponding to the rate k. $Cp^*RhP(OMe)_3(C_2H_4)(C_2H_5)^+$ (**7a**): k(23 °C) = 2.0 × 10^{-4} s^{-1}; $\Delta G^\ddagger$ = 22.4 kcal/mol. $Cp^*RhPMe_3(C_2H_4)(C_2H_5)^+$ (**7b**): k(23 °C) = 3.0 × 10^{-5} s^{-1}; $\Delta G^\ddagger$ = 23.4 kcal/mol. $CpRhP(OMe)_3(C_2H_4)(C_2H_5)^+$ (**8a**): k(23 °C) = 4.7 × 10^{-5} s^{-1}; $\Delta G^\ddagger$ = 23.4 kcal/mol. For complex $CpRhPMe_3(C_2H_4)(C_2H_5)^+$ (**8b**), after one turnover in the presence of an excess of ethylene, a new ethylene complex begins to grow in (presumably $CpRhPMe_3(C_2H_4)(C_4H_9)^+$). Since this depletes the concentration of catalyst, the best rate for the migratory insertion reaction is obtained by plotting data in the 0–1 turnover range: k(23 °C) = 4.1 × 10^{-6} s^{-1}; $\Delta G^\ddagger$ = 24.7 kcal/mol.

B. Dimerization Followed by GC (for 8). 2-Methylbutane was used as an internal standard in the GC analysis of butenes. Typically, a Schlenk flask was charged with the catalyst precursor and 4 equiv of internal standard. $CpRhPMe_3(C_2H_4)H^+$ (**4b**) (56.3 mg, 0.16 mmol) was dissolved in CH_2Cl_2 (ca. 15 mL) under an atmosphere of ethylene at 0 °C; $CpRhP(OMe)_3(C_2H_4)H^+$ (**4a**) was generated in situ from protonation of $CpRhP(OMe)_3(C_2H_4)$ (**2a**) (49.3 mg, 0.15 mmol) in CH_2Cl_2 at 0 °C. The solutions were warmed to ambient temperature (23 °C), and the dimerization reaction was then monitored by GC. Samples were taken at regular intervals and directly injected into the GC apparatus. Control experiments were run to insure that no metal-catalyzed isomerization was occuring in the GC port: during the dimerization reaction 1-mL samples were withdrawn and the volatiles (CH_2Cl_2 and butenes) vacuum transferred away from the metal. GC analyses of these volatiles were identical to the ones run in the presence of the metal complex. $CpRhP(OMe)_3(C_2H_4)(C_2H_5)^+$ (**8a**): k(23 °C) = 4.3 × 10^{-5} s^{-1}; $\Delta G^\ddagger$ = 23.4 kcal/mol. $CpRhPMe_3(C_2H_4)(C_2H_5)^+$ (**8b**): k(23 °C) = 3.3 × 10^{-6} s^{-1}; $\Delta G^\ddagger$ = 24.7 kcal/mol.

Generation and NMR Characterization of [$CpRhP(OMe)_3(\eta^3$-crotyl)$^+$][BF_4^-] 11 and 12. $CpRhP(OMe)_3(C_2H_4)$ (**2a**) (85 mg, 0.27 mmol) was dissolved in 7 mL of methylene chloride and cooled to −30 °C. $HBF_4{\cdot}Me_2O$ (1.3 equiv, 0.35 mmol) was syringed slowly into the solution. The solution was then exposed to an atmosphere of 1-butene and allowed to reach room temperature. The system was closed and left at ambient temperature for 6 days; the remaining solvent was then removed under reduced pressure to yield a brown oily residue. The residue was washed twice (2 × 3 mL) with hexane to eliminate any neutral species and identified as **11** (major) and **12** (minor) on the basis of ^1H and ^{13}C NMR. Complete NMR data are given only for the major isomer; the minor isomer was not present in sufficient quantities to clearly establish its spectral data. The structure of the major isomer was verified by X-ray analysis.[34]

NMR Data for [$CpRhP(OMe)_3(\eta^3$-crotyl)$^+$][BF_4^-] (11): ^1H NMR (CD_2Cl_2, 250 MHz, 23 °C) δ 5.68 (d, J_{RhH} = 2 Hz, C_5H_5), 5.24 (dt, J_{H4H2} = J_{H1H2} = 11 Hz, J_{H3H2} = 7 Hz, H_2), 3.93 (d, J_{H2H3} = 7 Hz, H_3), 3.72 (d, J_{PH} = 12 Hz, $P(OMe)_3$), 3.38 (m, H_1), 2.13 (dd, J_{H2H4} = 11 Hz, J_{RhH4} or J_{PH4} = 11 Hz, H_4), 1.85 (d, ^3J = 6 Hz, CH_3); ^{13}C NMR (CD_2Cl_2, 100 MHz, 23 °C) δ 91.2 (dd, J_{CRh} = 4 Hz, J_{CH} = 186 Hz, C_5H_5), 87.5 (dd, J_{CRh} or J_{CP} = 7 Hz, J_{CH} = 185 Hz, $CH_2CHCHCH_3$), 74.8 (ddd, J_{CRh} and J_{CP} are either 4 and 8 Hz or 8 and 4 Hz, respectively, J_{CH} = 158 Hz, $CH_2CHCHCH_3$), 53.7 (dq, J_{CP} = 4 Hz, J_{CH} = 150 Hz, $P(OCH_3)_3$), 45.5 (ddt, J_{CRh} and J_{PC} are either 5 and 11 Hz or 11 and 5 Hz, respectively, J_{CH} = 163 Hz, $CH_2CHCHCH_3$), 22.7 (q, J_{CH} = 130 Hz, $CH_2CHCHCH_3$).

Partial ^1H NMR Data for [$CpRhP(OMe)_3(\eta^3$-crotyl)$^+$][BF_4^-] (12): ^1H NMR (CD_2Cl_2, 250 MHz, 23 °C) δ 4.94 (dt, J_{H4H2} = J_{H1H2} = 11 Hz, J_{H3H2} = 6 Hz, H_2), 1.8 (d, ^3J = 6 Hz, CH_3).

Acknowledgment. This work was supported by the National Science Foundation (CHE-8705534). We thank Dr. D. L. Harris for assistance with the DNMR3 program, Dr. N. J. Pienta for help with error analyses, and Johnson-Matthey for a loan of $RhCl_3$.

(34) Brookhart, M.; Hauptman, E.; White, P. S. Unpublished results.